Surface energy and surface proton order of the ice Ih basal and prism surfaces

Surface energy and surface proton order of the ice Ih basal and prism surfaces

Ding Pan[1,2]**, Li-Min Liu**[2,3]**, Gareth A Tribello**[3,4]**, Ben Slater**[3,4]**, Angelos Michaelides**[2,3] **and Enge Wang**[1]

[1] Institute of Physics, Chinese Academy of Sciences, PO Box 603, Beijing 100190, People's Republic of China
[2] London Centre for Nanotechnology, University College London, London WC1H 0AJ, UK
[3] Department of Chemistry, University College London, London WC1H 0AJ, UK
[4] Davy Faraday Research Laboratory, University College London, Kathleen Lonsdale Building, Gower Street, London WC1E 6BT, UK

E-mail: angelos.michaelides@ucl.ac.uk

Abstract

Density-functional theory (DFT) is used to examine the basal and prism surfaces of ice Ih. Similar surface energies are obtained for the two surfaces; however, in each case a strong dependence of the surface energy on surface proton order is identified. This dependence, which can be as much as 50% of the absolute surface energy, is significantly larger than the bulk dependence ($<1\%$) on proton order, suggesting that the thermodynamic ground state of the ice surface will remain proton ordered well above the bulk order–disorder temperature of about 72 K. On the basal surface this suggestion is supported by Monte Carlo simulations with an empirical potential and solution of a 2D Ising model with nearest neighbor interactions taken from DFT. Order parameters that define the surface energy of each surface in terms of nearest neighbor interactions between dangling OH bonds (those which point out of the surface into vacuum) have been identified and are discussed. Overall, these results suggest that proton order–disorder effects have a profound impact on the stability of ice surfaces and will most likely have an effect on ice surface reactivity as well as ice crystal growth and morphology.

S Supplementary data are available from stacks.iop.org/JPhysCM/22/074209/mmedia

(Some figures in this article are in colour only in the electronic version)

1. Introduction

Ice Ih is the most common crystalline form of ice on earth. As such, the surfaces of ice Ih crystals are central to a wide variety of natural phenomena. For example, chemical reactions catalyzed on the surfaces of ice particles play a key role in the seasonal size variations of the southern hemisphere ozone hole [1]. The relative attachment rates of water molecules to the basal and prism faces of ice Ih dictate the structure (and beauty) of snow crystals and the morphology of crystals in stratospheric clouds [2]. In addition the widely discussed pre-melting of ice surfaces which is an everyday phenomenon that makes ice surfaces slippery and is crucial to ice skating, skiing and snow ball formation (see, e.g. [3, 4]).

The question of ice surface pre-melting has been widely debated since the time of Faraday [5]. However, much

less attention has been directed at the structure of ice surfaces at temperatures below the onset of pre-melting, either experimentally [6–10] or theoretically [11–13]. Determining ice Ih surface structure for even the simplest unreconstructed basal surface is a challenge because ice Ih is a proton disordered solid. This means that the ice Ih crystal can be considered as being built from a regular hexagonal arrangement of O atoms decorated quasi-randomly with protons within the constraints of a set of rules known as the Bernal–Fowler–Pauling ice rules [14, 15]. Unlike in bulk ice Ih, where the issue of proton order versus disorder has been widely discussed [16–18], understanding of the energetics of proton order at the surface is in its infancy [9, 11–13]. The presence of the surface raises interesting questions related to the issue of proton order versus disorder. For example, does the ice Ih surface retain the same degree of proton disorder as
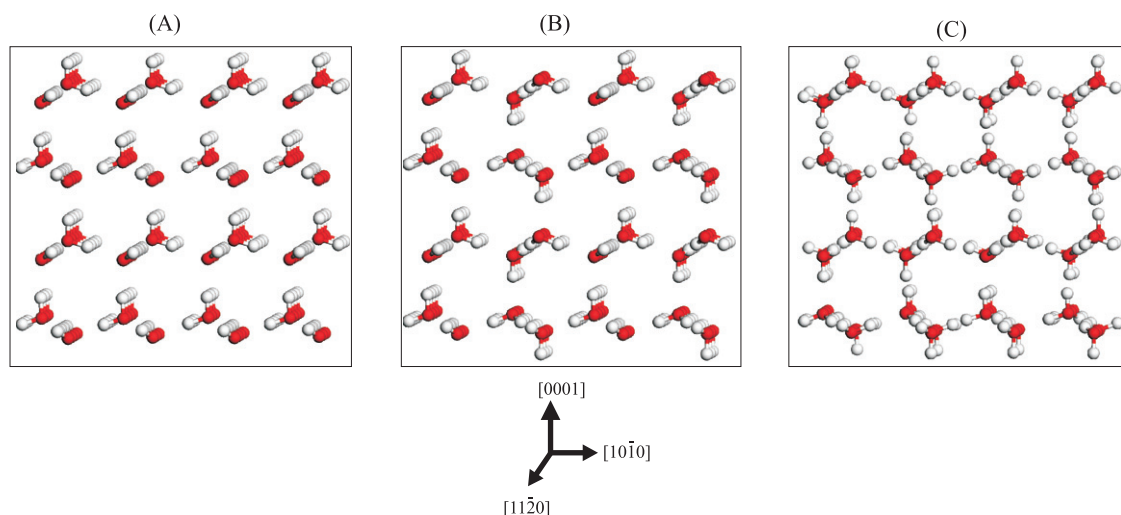
(A)   (B)   (C)

[0001]

[10$\bar{1}$0]

[11$\bar{2}$0]

Figure 1. Some 96 molecule bulk ice XI and ice Ih simulation cells. (A) Ferroelectric ice XI; (B) anti-ferroelectric ice XI; (C) an ice Ih structure. Red spheres represent the oxygen atoms and white spheres the hydrogen atoms.

in the bulk or does the presence of the surface introduce more or less disorder? Will the ice surface undergo an order–disorder transition along with the bulk order (ice XI) to disorder (ice Ih) transition at about 72 K?

Fletcher [11] appears to have been the first person to consider the question of proton disorder at ice Ih surfaces, tackling the question theoretically with intuitive heuristic models based on classical electrostatics. This led to the suggestion in 1992 that the low energy structure for the unreconstructed ice Ih basal surface should be proton ordered [11]. This conclusion was arrived at simply on electrostatic grounds by considering dipole interactions among nearest neighbor dangling OH bonds. Fletcher further suggested that this phase would transform in to a proton disordered state at about 30 K. Likewise the prism surface was predicted to be proton ordered with an order–disorder transition temperature of 70 K, close to the bulk order–disorder transition temperature of about 72 K. More recently, Buch *et al* used empirical potentials to compare basal faces with different proton arrangements [12]. Again proton ordered surfaces were predicted to be more stable than disordered ones with Fletcher's phase with alternating rows of dangling OH groups suggested to be the most stable. At a similar time we reported an *ab initio* determination of the surface energy of the basal surface of ice Ih along with a detailed consideration of the energetics of different proton arrangements [13]. Consistent with the studies of Fletcher and Buch *et al* our *ab initio* calculations predicted low total energy surfaces that were considerably more ordered than the bulk. In the present paper we now report a full account of this previous letter [13], expanded substantially to include results from other density-functional theory (DFT) exchange–correlation (xc) functionals, a 2D Ising model representation of the ice basal surface, and DFT results from the prism surface. The key conclusions from this study are that the range of energies spanned by typical proton ordered configurations is more than an order of magnitude larger than in bulk ice, implying a much higher order–disorder transition temperature at the surface

compared to the bulk. Monte Carlo (MC) simulations with parameterized potentials and solution of a 2D Ising model support this suggestion, predicting that the order–disorder transition, which occurs in the bulk at about 72 K, will not occur at the surface at any relevant temperature, i.e., not below the onset of surface pre-melting. Finally, the 'order parameter' introduced in our previous letter is discussed in detail and extended to predict relative surface energies of the prism surface with different proton arrangements.

This paper is organized as follows. Section 2 describes the methods used. The properties of bulk ice Ih/XI are discussed in section 3 as well as the ice models employed. The surface energies of the basal plane of ice Ih/XI are reported in section 4, and the order parameter that can rationalize the dependence of surface energy on proton order is defined in section 5. The order–disorder phase transition is discussed in sections 6 and 7 and in section 8 we extend our DFT calculations to the prism face. Finally, we close with a brief discussion and some conclusions in section 9.

2. Methods

DFT calculations have been performed with the CP2K/Quickstep program, which employs a hybrid Gaussian and plane-wave (GPW) basis set [19]. Two of the most popular generalized-gradient approximation (GGA) functionals for water/ice systems, namely Perdew–Burke–Ernzerhof (PBE) [20] and Becke–Lee–Yang–Parr (BLYP) [21–23], have been employed. Both functionals have been shown to describe the hydrogen bonds between water molecules reasonably well, and are able to reproduce hydrogen bond strengths between water molecules in small water clusters (water dimer to hexamer) to within 40 meV/water of the results obtained with second order Møller–Plesset perturbation (MP2) theory at the complete basis set limit [24, 25]. Core electrons are described with norm conserving Goedecker, Teter, and Hutter (GTH) pseudopotentials [26], with the wavefunctions of the valence electrons expanded in terms of Gaussian functions with a triple-ζ

doubly polarized basis set (TZV2P). Convergence tests are also reported with a larger quadruple-ζ doubly polarized basis set (QZV2P). For the auxiliary basis set of plane waves a 340 Ryd density cut-off is used. During the geometry optimization, all atoms in the supercell are fully relaxed. For bulk calculations, cells with at least 96 water molecules were employed (figure 1) and for surface calculations a variety of surface structural models were used, with between 8 and 48 waters per bilayer. The smallest unit cells with 8 water molecules per bilayer have 2×1 orthorhombic periodicity and the largest unit cells have 4×3 periodicity, as illustrated in figure 4. In some convergence tests up to 15 bilayer thick slabs were used, however, as we will show below the surface energy of the basal surface is rather insensitive to the number of bilayers used and is already converged for 2–3 bilayer thick slabs. The vacuum spacing between slabs is at least 20 Å thick, and Brillouin zone k-point sampling has been limited to the Γ point only.

As well as DFT, some calculations with empirical potentials are reported, in particular MC simulations on the question of an order–disorder transition at the basal surface. The empirical potential used is a six site, rigid body, potential due to Nada and van der Eerden (NvdE) [27] but modified so that it reproduces the DFT proton ordering energies of designated proton configurations. The ice melting temperature for this potential model is approximately 285 K [28] and it has been used to study crystallization [29] and more recently pre-melting [30] of ice crystal surfaces. More details on the construction and performance of the potential can be found in the supplementary information (available at stacks.iop.org/JPhysCM/22/074209/mmedia). In the MC simulations only proton rearrangements were considered and the oxygen atoms were fixed at their ideal lattice sites. Slabs with a minimum thickness of 6 bilayers and 160 molecules per bilayer were used. Using a modification of the algorithm due to Rick *et al* [31], on each MC trial move, a sequence of protons are reoriented within a 'loop' of hydrogen bonds which either run from surface to opposing surface or from the surface into the bulk and back to the starting surface. The energy is evaluated and the move is accepted subject to Metropolis sampling. All simulations were run for at least 500 000 steps, and the mean and variance data was collected over the final 15 000 accepted moves.

3. Bulk ice

In this section we discuss our results for bulk ice Ih and ice XI. First we briefly present some results from basis set and xc functional tests and then focus on the energetics of different proton ordering configurations.

Two exchange–correlation functionals, PBE and BLYP, have been tested on a ferroelectric ice XI model. Table 1 shows that PBE predicts a larger (17%) lattice energy than BLYP, with the experimental value excluding zero point energy between the two. Upon moving from the TZV2P to the QZV2P basis sets the absolute lattice energy is reduced by about 30 meV/H_2O. Along with the difference in lattice energies, PBE predicts a 5.7% smaller volume per water than BLYP. Recently, Feibelman [32] reported plane-wave results

Table 1. For a 96 molecule ice XI supercell, two xc functionals and two basis sets are tested. Energy–volume data is fitted to a Murnaghan equation of state to obtain the equilibrium volume and bulk modulus. The experimental results for the volume and cohesive energy at 10 K are taken from [38, 39], while the experimental bulk modulus comes from [40] at 257 K.

xc, basis set	Volume (Å^3/H_2O)	Cohesive energy (meV/H_2O)	Modulus (Mbar)
PBE, TZV2P	30.54	−706	0.15
PBE, QZV2P	30.73	−678	0.15
BLYP, TZV2P	32.34	−598	0.17
BLYP, QZV2P	32.48	−569	0.17
Experiment (10 K)	32.05 [38]	−610 [39]	0.09 [40]

for these two functionals (using an 12 molecule 'ice Ih' unit cell[5]) and obtained similar trends: PBE tends to overestimate the strength of the hydrogen bonds in ice bulk, while BLYP gives weaker hydrogen bonds. Feibelman calculated a lattice energy of 640 meV/H_2O with PBE and 520 meV/H_2O with BLYP, values that are a little smaller than our QZV2P values, 676 and 567 meV/H_2O. Differences are most likely due to basis set incompleteness errors in the local Gaussian orbitals used here.

Let us now discuss the various proton disordered configurations representative of ice Ih. Correctly representing the quasi-random arrangement of the protons is a challenge for computer simulations, as calculations are confined to a finite simulation cell and employ periodic boundary conditions to mimic the infinite solid. For simulations of ice Ih the finite cell should be sufficiently large to capture the randomness of the proton arrangements and should also minimize multipole moments of the charge distribution so as to avoid long-range interactions between cells. This is achieved here with moderately large 96 molecule unit cells within which random ice configurations are generated by Cota and Hoover's method [33], as further developed by Hayward and Reimers [34] (Hayward and Reimers' so-called C2 constraint). A fully coordinated water molecule forms 4 hydrogen bonds. As each water molecule has two identical hydrogen atoms, there are six different orientations it may have. The C2 constraint ensures that each water molecule orientation appears the same number of times within each bilayer. This constraint ensures that each bilayer of ice Ih has zero net dipole moment, which is convenient when building slab models with different thicknesses.

We have built and tested 21 ice Ih structures that satisfy the C2 constraint and have also tested the 16 different symmetry-unique structures of an 8 molecule orthorhombic unit cell [18]. The distribution of lattice energies in ice Ih and ice XI is shown in figure 2. Of all the 37 structures with different proton orientations, ice XI has the lowest bulk energy, which is consistent with previous DFT studies [18, 35]. We find that the lattice energies for all of the ice structures

---

[5] Note that the distinction between ice XI (ferroelectric and anti-ferroelectric) and the highly ordered 'ice Ih' one necessarily gets when a small, e.g. 12 molecule, unit cell is used is often unclear. Indeed ferroelectric and anti-ferroelectric ice XI models are often referred to as ice Ih (see, e.g. Hirsch and Ojamäe's work [18]).
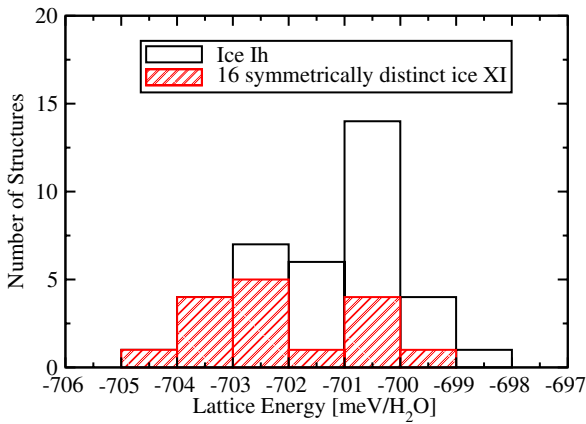
Figure 2. Distribution of ice Ih lattice energies with different proton arrangements. All data in the histogram has been obtained in 96 molecule unit cells fixed at a volume of 32.05 Å^3/H$_2$O. The PBE xc functional and a TZV2P basis set has been used.

Figure 3. Top views of the (0001) basal plane of ice Ih. (A) A ball and stick representation of three hexagons in the top bilayer. The green hexagon identifies the 6 nearest neighbor positions to the dangling OH in the center at which other dangling OH bonds may be present. In this particular structure 3 out of the 6 nearest neighbor sites have a dangling OH group, yielding $c_i = 3$ for the central dangling OH. (B) A proton disordered ice Ih surface. (C) A proton ordered ice Ih surface. Red spheres are oxygen atoms and white ones are hydrogen atoms. In order to emphasize the proton distribution of the dangling OH groups more clearly the atoms in (B) and (C) are increased in size.

examined have energies within 5 meV/H$_2$O. Thus proton order versus disorder effects do not have a major impact on the lattice energy of the crystal, which again is in agreement with previous DFT studies performed for smaller simulation cells [18, 35].

The energy difference on the level of $\leqslant 5$ meV/H$_2$O between the lowest energy ordered ice XI structure and the disordered ice Ih structures is in the right ballpark for a bulk order–disorder transition of about 72 K. At the ice XI–Ih phase transition temperature (T), the ordering energy ΔE should equal $T\Delta S$, where ΔS is the entropy difference between the ordered (ice XI) and disordered (ice Ih) phases. In this system the entropy is comprised of two parts: vibrational and configurational entropy. The vibrational entropy differences between the two phases is expected to be almost negligible since the phonon frequencies of ice XI and Ih do not differ greatly, as has been seen through comparison of calculated phonon dispersion curves of ice XI with experimental phonon dispersion curves of ice Ih [36, 37]. Thus the phase transition temperature is governed primarily by differences in configurational entropies, something which Pauling has shown to be given by $S^{\text{conf}} = k_B \ln(\frac{3}{2}) = 0.035$ meV/(K·H$_2$O) [15]. Hence at the phase transition temperature, the configurational entropy contributes 2–3 meV/H$_2$O, which is consistent with the $\leqslant 5$ meV/H$_2$O total energy difference between the two phases. Therefore these reference calculations of bulk lattice energy demonstrate that DFT approaches are appropriate for tackling the subtle question of proton order and disorder in ice. Indeed, the verity of this approach was demonstrated already by Knight *et al* [17] who neglected the vibrational contribution to the entropy and predicted a bulk transition temperature of ca. 100 K based on DFT calculations.

4. Basal surface

We now discuss the (0001) basal plane of ice XI/Ih (see figures 3 and 4), focusing mostly on the surface energy. The surface energy is a key thermodynamic quantity of any surface,
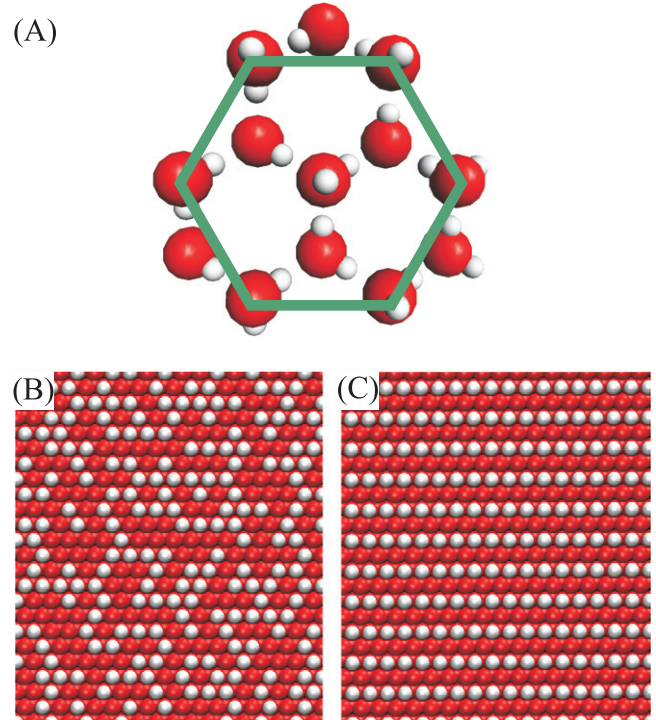
since it affects crystal growth and controls the equilibrium crystal shape. Experimentally the surface energy of ice can be estimated by measuring the contact angle of a water drop on a solid ice surface. Notionally this technique provides the interface energy between ice and vapor however little is known about how the ice surface structure is changed in the vicinity of the water drop, which is important as the formation of some intermediate structure might affect any surface energy estimate. Makkonen [41] observed that the value for the contact angle between a hot water drop (95 °C) and the ice surface is 37°, and so estimated the interface energy of ice to be roughly 4.8 meV Å^{-2} (77 mJ m^{-2}) at −25 °C. Many empirical and semi-empirical methods have been employed to calculate the surface energy but the results strongly depend on the model and the parameters (see, e.g. [42–45]) and so literature estimates span a large range of values, from 4.3 to 18.6 meV Å^{-2}. Therefore, obtaining the surface energy of ice at the atomic scale using an *ab initio* approach is worthwhile.

The surface energy γ is calculated throughout in this paper as:

$$\gamma = \frac{E_{\text{tot}}^{\text{slab}}(n) - n E_{\text{tot}}^{\text{bulk}}}{2A}, \qquad (1)$$

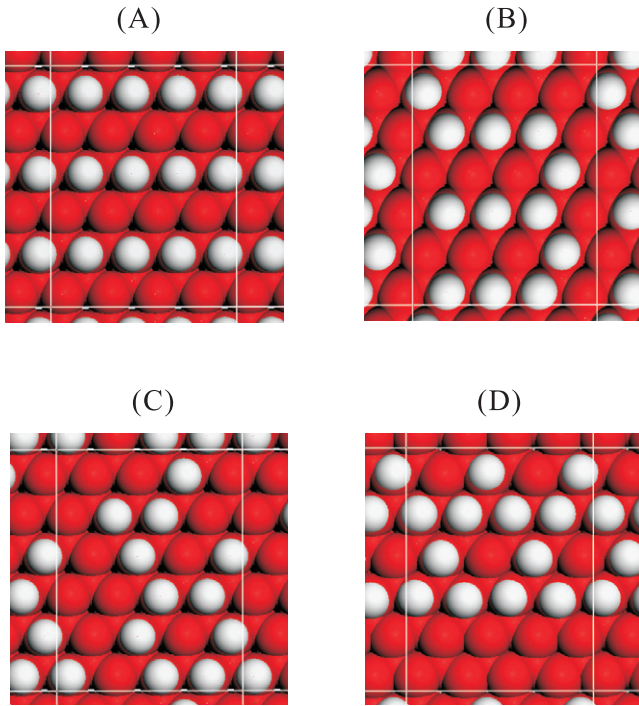where $E_{\text{tot}}^{\text{slab}}$ is the total energy of the ice slab obtained from our

(A)   (B)

(C)   (D)

Figure 4. Top view of the (0001) basal plane of ice Ih with order parameters C_{OH}^B, (A) and (B) 2.00, (C) 2.67 and (D) 3.33. Red balls for O and white balls for H are enlarged here to distinguish the proton arrangement at each surface. The 4×3 unit cell (with 48 water molecules per bilayer) is indicated in each figure.

Figure 5. (A) DFT PBE surface energies of 16 different ice Ih basal surfaces. The reference bulk lattice energies associated with each of the distinct ice Ih slabs are also given (blue data and right axis). Compared to the large range of surface energies, the range of energies in the bulk is very small. In order to compare them directly, equivalent units are used for both the surface and lattice energies. (B) Surface energies of the ice Ih/XI structures in figure 4 (structures (A), (C), and (D)) as a function of the number of bilayers in the slabs. Results for PBE and BLYP are reported. (C) Correlation between surface energy and order parameter, C_{OH}^B, with PBE, BLYP and the modified NvdE potential.

DFT calculations, n is the number of bilayers in the slabs, and A is the surface area of each side of the slab. The bulk reference per molecular bilayer, E_{tot}^{bulk}, is extracted from calculations on ice slabs from the relation:

$$E_{tot}^{bulk} = E_{tot}^{slab}(n) - E_{tot}^{slab}(n-1), \qquad (2)$$

where, as before, n is the number of bilayers in the slab. This relation is valid because, for slabs thicker than some critical thickness, the bilayer insertion energy is equivalent to the addition of a bilayer of bulk ice. In order to achieve good convergence with the number of bilayers we used identical simulation cells and identical fast Fourier transform (FFT) grids for each calculation so that a high numerical precision was ensured.

The surface energy has been computed for anti-ferroelectric ice XI. (Consistent with previous studies, and because it possesses a dipole moment along the surface normal the ferroelectric ice XI surface is unstable [12, 46, 47].) We find that, for the surfaces examined, γ is rather insensitive to the number of layers used in the calculations and is already converged for slabs of 2–3 bilayers thick (figure 5). Here the surface energy of the 3 bilayer ice XI slab is within 0.2 meV Å^{-2} of the thickest 6 bilayer slab computed. Similar behavior is observed for anti-ferroelectric ice XI for which slabs up to 15 bilayers thick were tested. The PBE surface energies for the ice XI slab are generally about 17% larger than those obtained with BLYP (figure 5), which is consistent with the difference of lattice energies
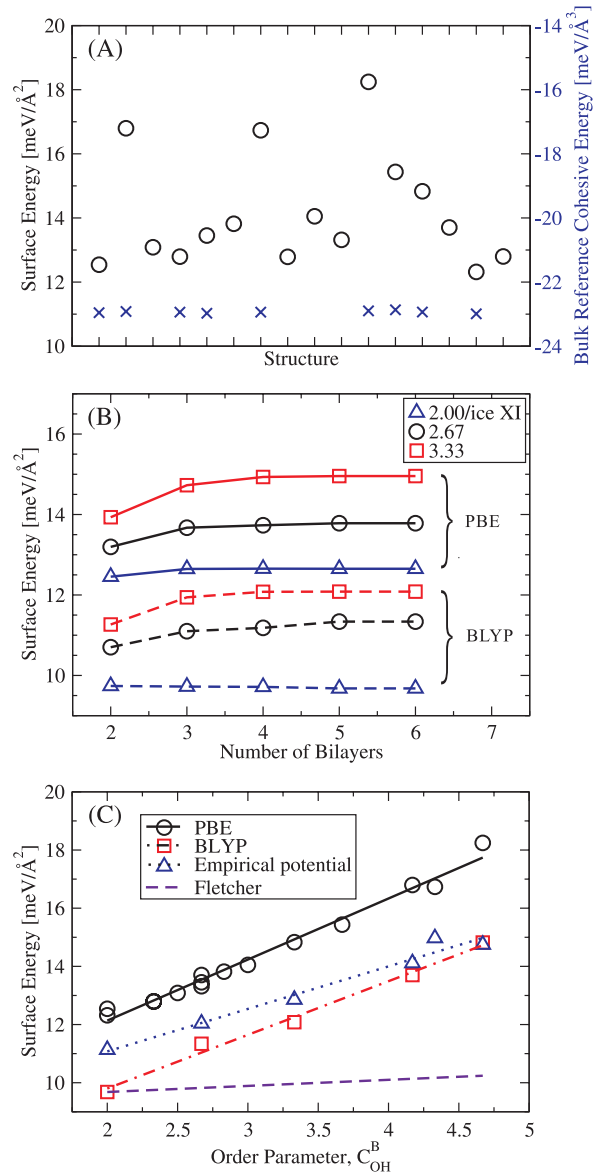
with these two exchange–correlation functionals. A value of 12.2 meV Å^{-2} (206 meV/(H_2O in top half bilayer)) is obtained with the PBE xc functional for the basal plane, while BLYP gives 9.7 meV Å^{-2} (171 meV/(H_2O in the top half bilayer)). Because for the bulk calculation, the experimental cohesive energy of ice XI lies between the PBE and BLYP results, we speculate that the actual value for the surface energy of the basal plane for anti-ferroelectric ice XI is between these

two values:

$$9.7 \text{ meV Å}^{-2} < \gamma_{XI}^{B} < 12.2 \text{ meV Å}^{-2}, \qquad (3)$$

where the superscript B is used to refer to the basal surface. The absolute value of the surface energy obtained here is not much more than the energy needed to break one hydrogen bond per water molecule in the top half bilayer. Specifically, recalling that the lattice energy with PBE and a TZV2P basis set is 706 meV/H_2O and that each water in bulk ice has four hydrogen bonds, then a single hydrogen bond in bulk ice is equivalent to 177 meV/H_2O, which is not far from the 206 meV/(H_2O in top half bilayer) value for the surface energy obtained. This also suggests that surface relaxation effects are small.

For ice Ih a unique value for γ_{Ih}^{B} is not obtained. Instead a range of values is observed, from 12.2 meV Å^{-2} (206 meV/(H_2O in top half bilayer)) to 18.2 meV Å^{-2} (308 meV/(H_2O in top half bilayer)) from PBE, at the lower end of this range is the anti-ferroelectric ice XI structure (see figure 5). The fact that we do not get a unique value for ice Ih is to be expected since, as we know, the lattice energy of bulk ice depends on the degree of proton disorder within the simulation cell. The interesting finding here is that the variations in surface energy for configurations which differ only in the degree of proton order by far exceeds the small range of energies found in bulk (see figure 5). Specifically, for the structures considered in figure 4, variations in proton order cause differences in the bulk energy of less than 1% (about 5 meV/H_2O) whereas the dependence of surface energy on proton order can be as much as 50% (about 100 meV/(H_2O in top half bilayer).) This implies that there will be insufficient thermal energy available to allow entropy to disorder the surface at any relevant temperature—that is to say any temperature below the onset of surface melting. This qualitative conclusion is reinforced later in the paper with the aid of Monte Carlo simulations and Ising model calculations.

Although there is a large range of energies for the different ice surface structures, the O–O lengths in the surface bilayer do not change much compared to those in the bulk. The average O–O distance in the surface bilayer is 0.02 Å larger than in the bulk for the different ice Ih surfaces considered. This is consistent with the experimental change of 0.01 Å (2.77 Å for surface and 2.76 Å for bulk) measured at 38 K [10]. However, we notice that on many surfaces adjacent dangling OH bonds on the surface often move away from their initial upright positions so as to 'lean' away from each other as much as possible. This suggests that there is a repulsive force between the dangling OH bonds at the surface, and it is this force which is believed to be responsible for the large range of ice Ih surface energies.

5. Order parameter on basal surfaces

We now try to understand the large range of values for γ_{Ih}^{B}. As discussed briefly in section 1, previous work of Fletcher [11] and Buch *et al* [12] (as well as work on water clusters [48]) has shown that the upright OH groups, those which 'dangle'

out of the surface, play an important role in determining the energetics of the surface. An analysis of our DFT data supports this suggestion and, indeed, we find that the spatial distribution of the dangling OHs is key to the observed range of surface energies.

In order to distinguish different distributions of dangling OH bonds we define an order parameter on the basal plane:

$$C_{OH}^{B} = \frac{1}{N_{OH}} \sum_{i=1}^{N_{OH}} c_i, \qquad (4)$$

where N_{OH} is the total number of dangling OH bonds on the two surfaces of our simulation slab and c_i is the number of nearest neighbor, dangling OH bonds around the ith dangling OH bond (see figure 3). Note that the nearest neighbor site for one dangling OH group beside another corresponds to the second nearest neighbor site of the hexagonal O lattice. This order parameter, C_{OH}^{B}, quantifies the average separation between the dangling OH groups at the surface: the larger the value of C_{OH}^{B}, the more inhomogeneous the distribution of the dangling OH groups is with the consequence that on average the dangling OH groups at the surface are closer together. A fully random proton arrangement of dangling OH groups will, in principle, have a value of $C_{OH}^{B} \approx 3$. The smallest possible value of C_{OH}^{B} for a non-polar surface is 2, which conveniently and by construction corresponds to, amongst other structures, those resembling anti-ferroelectric ice XI surfaces (see figure 4). The upper limit for the order parameter is, in principle, 6; an unrealistic limit that would only be reached when the area of an ideal ice surface approaches infinity and the contribution of $c_i < 6$ sites at the edge of a $C_{OH}^{B} = 6$ patch is diminished.

We find that when the surface energies extracted from the calculations of the many surfaces considered are plotted as a function of C_{OH}^{B}, a linear relationship is obtained: as C_{OH}^{B} increases so too does γ_{Ih}^{B}. This relation holds for PBE, BLYP and also the modified NvdE potential used. The absolute values of the surface energies calculated using the empirical potential are between BLYP and PBE, however, its slope is a little smaller than that obtained from the DFT calculations, as shown in figure 5(C). It can also be seen that the lowest energy surfaces are those with an order parameter, $C_{OH}^{B} = 2$. The fact that this is a true surface effect can be further seen by the absence of a dependence of C_{OH}^{B} on the bulk energies extracted from each slab using equation (2). For the lowest value of the order parameter, $C_{OH}^{B} = 2$, we have computed 6 structures which with PBE all have surface energies within 0.5 meV Å^{-2} or 8 meV/(H_2O in top half bilayer). Some of these $C_{OH}^{B} = 2$ surfaces correspond to Fletcher's striped phase (e.g. (A) in figure 4) and some do not (e.g. (B) in figure 4). Therefore, although it is clear at this stage that the lowest energy surfaces are those with $C_{OH}^{B} = 2$, it is not yet prudent to designate any one particular termination as 'the' lowest energy structure of the ice surface. Indeed more subtle effects, e.g. second nearest neighbor interactions of dangling OH bonds or the orientations of the non-dangling OH bonds at the surface, are likely to be important in this regard. To investigate these effects would require unit cells with much larger lateral dimensions than those considered here.

Can the physical origin of the strong dependence of γ_{Ih}^{B} on the proton arrangement at the surface be understood more clearly? To answer this a classical electrostatics model proves useful. The surface energy of ice Ih (1) can be rewritten as,

$$\gamma_{Ih}^{B} = R + E_{HH}/2A, \qquad (5)$$

where R comprises all energy contributions apart from the repulsion energy E_{HH} between the dangling OH groups. Expanding (5) we obtain:

$$\gamma_{Ih}^{B} = R + \frac{1}{2} \sum_{\substack{i,j \\ i \neq j}}^{N_{OH}} \frac{q_i q_j}{r_{ij} 2A} \Theta(r_{ij}), \qquad (6)$$

where, q_i is the 'effective charge' on the H atom of the ith dangling OH, r_{ij} is the distance between the ith and jth dangling OHs, and $\Theta(r_{ij})$ gives the interaction range of this screened Coulomb potential. The sum runs over all the N_{OH} dangling OH bonds. Here, if we select a range for this interaction which includes only the nearest neighbor dangling OH bonds on the surface, then $\Theta(r_{ij})$ is

$$\Theta(r_{ij}) = \begin{cases} 1, & \text{if } r_{ij} \leqslant d_{HH} \\ 0, & \text{if } r_{ij} > d_{HH}. \end{cases} \qquad (7)$$

Considering equal 'effective charges' on the protons of the dangling OH groups we arrive at:

$$\gamma_{Ih}^{B} = R + \frac{1}{2} \sum_{i}^{N_{OH}} \frac{q^2}{d_{HH} 2A} c_i. \qquad (8)$$

Combining this with equation (4) we obtain

$$\gamma_{Ih}^{B} = R + \frac{q^2}{4 d_{HH} A} C_{OH} N_{OH}. \qquad (9)$$

If we define,

$$\sigma = \frac{A}{N_{OH}}, \qquad (10)$$

which is the average area of a water molecule in the top half bilayer ($\frac{1}{\sigma}$ is the surface density of water molecules in the top half bilayer) we arrive at:

$$\gamma_{Ih}^{B} = R + \frac{q^2}{4 d_{HH} \sigma} C_{OH}, \qquad (11)$$

or,

$$\gamma_{Ih}^{B} = \gamma_{Ih, C_{OH=2}}^{B} + \frac{q^2}{4 d_{HH} \sigma} (C_{OH}^{B} - 2) \qquad (12)$$

an expression for γ_{Ih}^{B} which depends linearly on C_{OH}^{B} with a slope proportional to q^2, where $\gamma_{Ih, C_{OH=2}}^{B}$ refers to the surface energy of ice Ih with the order parameter $C_{OH}^{B} = 2$. If d_{HH} is set to an average value of 4.42 Å for PBE or 4.55 Å for BLYP (taken from our computed nearest neighbor distances at the ice surface) and σ is 16.92 Å^2 for PBE and 17.68 Å^2 for BLYP, then the best fit value for the charge is a physically reasonable 0.21e for both PBE and BLYP[6]. This leads to

[6] The effective charge q in the empirical potential calculations is 0.17e, which is close to the DFT result.

good fits to the PBE and BLYP data as shown by the lines in figure 5(C). For the PBE calculation, the root mean square error of the fit is 3.7 meV/(H$_2$O in the top half bilayer), which is smaller than the spread in the DFT data at all given values of C_{OH}^{B}. Therefore, the energies of all the surfaces and thus the essential physics in these systems can be understood to first order by simple electrostatics governed by repulsion between the nearest neighbor dangling OH groups alone.

Before moving on to explore the details of a possible order–disorder phase transition at the basal surface, we consider why the energy is so much more sensitive to the arrangement of the protons at the surface than it is in the bulk. The key point, we suggest, is that the interactions between dangling OH bonds at the surface is governed by effective charge–charge interactions—as observed from the $1/d$ dependence of C_{OH}^{B} (figure 5(C))—whereas notionally dangling OH bonds in the interior of the crystal interact through a weaker dipole–dipole interaction. This reasoning follows Fletcher's suggestion that a fully coordinated water molecule in bulk ice can be regarded as consisting of four 'elementary dipoles', directed tetrahedrally along the directions of the two O–H bonds and the two lone pairs [11]. In bulk the elementary dipoles participating in hydrogen bonds to neighboring water molecules have small interaction energies. Indeed when Fletcher was addressing the tendency for dangling OH bonds to align at the surface it was discussed in terms of interactions between the elementary dipole of the dangling OH groups, rather than an effective charge interaction that we see here. Interactions between these elementary dipoles would lead to a much weaker dependence of the surface energy on C_{OH}^{B}, as indicated by the line labeled Fletcher in figure 5(c). This is the main reason why Fletcher predicted a much lower order–disorder transition temperature than our DFT results would suggest.

6. Monte Carlo simulations

Having arrived at a DFT description of the energetics of proton order at the surface of ice, and having demonstrated that the energetics of proton order differs significantly between the surface and the bulk, we now consider the implications of this result to the ice XI–Ih order–disorder transition. So as to access a large range of temperatures, including unrealistically high temperatures (up to 500 K) without the 'complications' of melting, structural relaxation effects such as displacements of the water molecules from their lattice sites are not considered, i.e., the focus is on proton reorientation and the influence this has on the free energies of the slabs. The results from the MC simulations are striking and summarized in table 2. The key conclusion is that at all temperatures below the melting point the surfaces maintain an order parameter close to $C_{OH}^{B} = 2$. Indeed upon passing through the bulk order/disorder transition temperature (72 K) no additional disorder at the surface is introduced so C_{OH}^{B} remains at precisely 2.00. Moreover, even at an unrealistically high temperature of 500 K (made possible in the MC simulations because the O lattice is fixed), the surface is still far from being fully disordered, possessing a value of only $C_{OH}^{B} = 2.33$. Thus even the thermal energy at 500 K is not sufficient to permit modestly high C_{OH}^{B} states to

Table 2. Variation of C_{OH} with temperature for an empirical potential that correctly describes the bulk and surface proton order energetics, as obtained from Monte Carlo sampling with a rigid oxygen lattice. The results are averaged over the two faces of a six layer slab and layer 1 corresponds to the external surface (top half bilayer). Layer 3 lies in the interior of the crystal. The average variance within each bilayer is given in parenthesis.

T (K)	Layer 1	Layer 2	Layer 3
40	2.00 (0.000)	2.42 (0.041)	2.44 (0.007)
100	2.00 (0.000)	2.48 (0.020)	2.58 (0.026)
125	2.01 (0.000)	2.55 (0.017)	2.69 (0.018)
150	2.04 (0.002)	2.63 (0.022)	2.74 (0.023)
200	2.13 (0.003)	2.70 (0.022)	2.75 (0.028)
500	2.33 (0.011)	2.71 (0.020)	2.74 (0.023)

be accessed. The MC simulations also permit us to examine how the ordering in specific bilayers varies as one descends into the bulk. From the data in table 2, it can be seen that, even by the second and third layers, considerably larger values of C_{OH}^B are observed.

7. The ice basal surface as a triangular Ising model

Fletcher's nearest neighbor approximation for the ice basal surface is equivalent to an anti-ferromagnetic Ising model of protons on a triangular lattice. We now use this correspondence to explore the details of a possible phase transition on the basal plane and the temperature dependence of C_{OH}^B. In 1950 Wannier famously solved the anti-ferromagnetic Ising model on a triangular lattice analytically, and proved that there is no order–disorder phase transition [49]. Although this strongly suggests that there will not be a phase transition, we cannot apply this conclusion directly here because of the additional constraint that there is no dipole moment perpendicular to the surface, that is $N/2$ of the N possible sites for protons at the surface must always be occupied. We therefore tackled this problem numerically with MC within the framework outlined briefly below. The key point, as we will show, is that in accordance with Wannier's analytic solution a phase transition is not observed. In addition we find that at all relevant temperatures the order parameter C_{OH}^B remains close to 2.

The occupation number, t_i, of a site for a proton is 0 for an empty site and 1 for an occupied site. With the help of a spin operator, σ_i,

$$t_i = \frac{\sigma_i + 1}{2}, \qquad (13)$$

where a spin of $+1$ indicates the presence of a H at the site and -1 corresponds to an unoccupied site. E_{HH} in (5) can now be rewritten as,

$$E_{HH} = \epsilon \sum_{n.n.} t_i t_j, \qquad (14)$$

where ϵ is the repulsive (i.e. 'anti-ferromagnetic') interaction energy of two nearest neighboring (n.n.) H atoms. Here we extract the nearest neighbor interaction from the fit to our PBE data with equation (12). For the honeycomb lattice examined the Hamiltonian is

$$H = \frac{\epsilon}{4} \sum_{n.n.} \sigma_i \sigma_j + \frac{3\epsilon}{2} \sum_i \sigma_i + \frac{3\epsilon N}{4} \qquad (15)$$
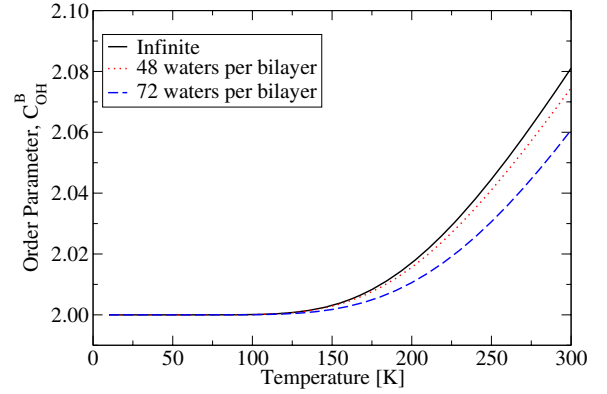

Figure 6. Order parameter versus temperature obtained from a triangular Ising model with nearest neighbor interactions taken from PBE. The black solid curve shows the result of Wannier's strict Ising model solution [49] and is to be compared with our simulation results with 48 (red dotted line) and 72 (blue dashed line) water molecules per bilayer.

and the canonical distribution gives the temperature dependence of the order parameter

$$\langle C_{OH}^B \rangle_T = \int_2^6 g(C_{OH}^B) C_{OH}^B \, e^{-\frac{E_{HH}(C_{OH}^B)}{k_B T}} \, dC_{OH}^B, \qquad (16)$$

where $g(C_{OH}^B)$ is the configurational density of states, that is, the number of configurations with a certain order parameter C_{OH}^B, and k_B is the Boltzmann constant.

The results of the numerical simulations obtained from MC simulations in periodic unit cells with the equivalent of 48 and 72 water molecules per bilayer are shown in figure 6, along with Wannier's solution (labeled 'infinite'). The curves show no singular points over the temperature range shown (or at any temperature investigated). In addition for the range of temperatures shown $C_{OH}^B \approx 2.0$; even at 300 K C_{OH}^B is still less than 2.1. Of course the Ising model results obtained here are consistent with the MC simulations in section 6, which also show that the surface remains at $C_{OH}^B \approx 2.0$ at all temperatures below the pre-melting temperature. We conclude therefore that an order–disorder transition, equivalent to the one in bulk ice which occurs at about 72 K, does not take place at the basal surface at any temperature before pre-melting occurs.

8. Prism surface

Let us now briefly consider the energetics of the prism $(10\bar{1}0)$ surface of ice Ih and ask if its energy also depends strongly on the spatial arrangement of the dangling OH bonds. As we did for the basal surface, we answered this question by using DFT (PBE) to compute the surface energies of a variety of surfaces with different arrangements of dangling OH bonds. Some important examples of structures considered are shown in figure 7 and the range of surface energies obtained for all the structures considered is given in figure 8. The key features to emerge from these studies are: (i) the lowest energy surfaces have surface energies of ca. 12.0 meV Å^{-2}, very similar to the surface energy of the lowest energy basal surface terminations
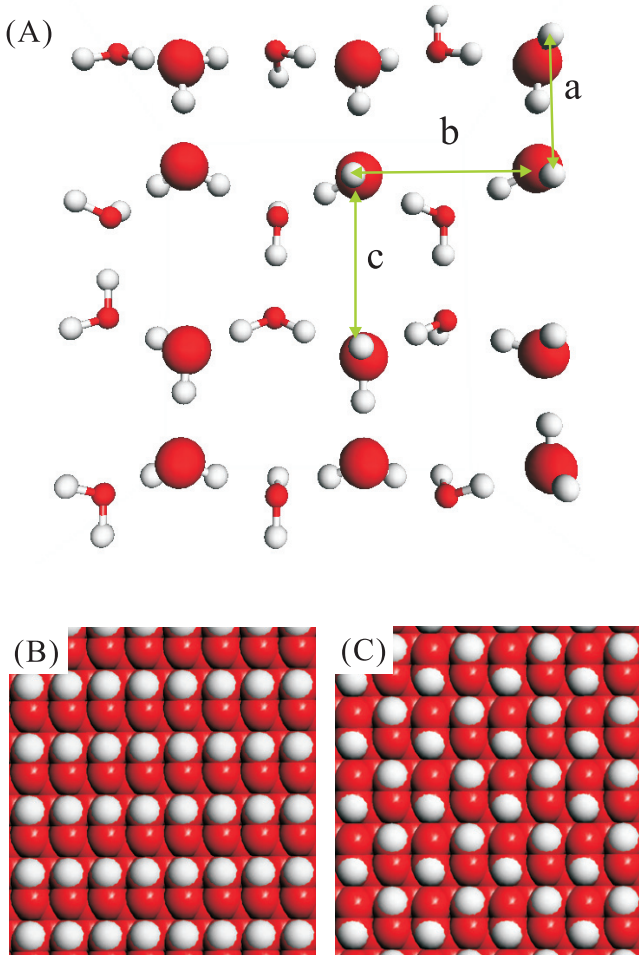
Figure 8. Relation between surface energy and the order parameter C_{OH}^P on the prism ($10\bar{1}0$) surface of ice Ih, as obtained with PBE and a TZV2P basis set.

Figure 7. Top views of the ($10\bar{1}0$) prism surface of ice Ih. In (A) the molecules in the top layer are shown larger for clarity and three different distances (a, b and c) between nearest neighbor dangling OH groups are indicated. (B) and (C) are the lowest order parameter surfaces of the prism surface using the order parameter, C_{OH}^P, defined in equation (4). Red balls for O and white balls for H are enlarged to distinguish the proton arrangement in (B) and (C).

(when computed with the same computational set-up). The structures of the two lowest energy surfaces identified are shown in figures 7(B) and (C). Structure (B) was predicted to be the lowest energy state by Fletcher [11]. However, according to our DFT PBE calculations, structure (C) has essentially the same energy as (B). (ii) A large range of surface energies has again been found, corresponding to as much as 50% of the absolute surface energy of the prism surface; (iii) the range in surface energies is again related to the arrangement of dangling OH groups and an order parameter to discriminate surfaces with different spatial arrangements of dangling OH bonds has been identified.

Since we again find that it is the interaction between dangling OH bonds that is the key to understanding the large range in surface energies, we can apply the same theoretical approach we applied to understanding the energetics of the basal face to understanding the energetics of the prism surface. However, there are some subtleties that must be taken into account in particular the fact that there are three different
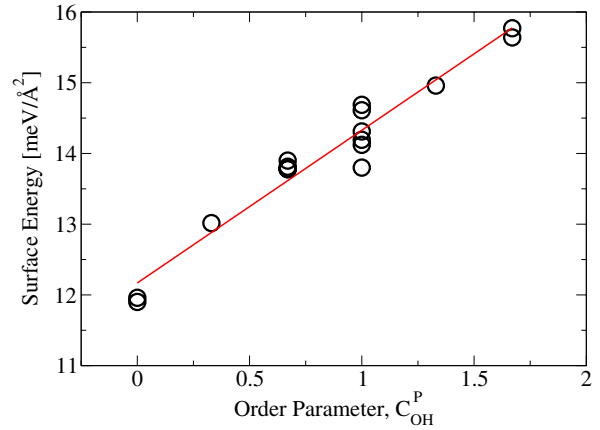
nearest neighbor dangling OH distances on the prism surface (these are designated a, b and c in figure 7). Furthermore, unlike the basal plane, on the prism surface the dangling OH bonds are not perpendicular to the surface. For simplicity, if the interaction range is set to a value of 4.00 Å, the Coulomb interaction between dangling OH bonds includes only interactions between hydrogens separated by distances a and c. The order parameter on the prism plane has the same form as equation (4):

$$C_{OH}^P = \frac{1}{N_{OH}} \sum_{i=1}^{N_{OH}} c_i \qquad (C_{OH}^P \in [0, 2)), \qquad (17)$$

where P refers to prism surfaces and c_i counts the number of nearest neighbor dangling OH bonds with the distances a or c around the ith dangling OH. With this definition of order parameter and cut-off in the interaction range, both structures (B) and (C) in figure 7 come out with the lowest order parameter $C_{OH}^P = 0$. In addition, the surface energies of all prism surfaces considered exhibit a clear dependence on C_{OH}^P and the best fit value for the effective charge on the protons of the dangling OH bonds on prism plane is $0.19e$, which is close to the value of $0.21e$ found for the basal plane. Thus overall we see that the spatial distribution of dangling OH bonds has a big impact on the energetics of the prism surface and much of the understanding arrived at in our studies of the basal surface carry over to the prism surface.

9. Discussion and conclusions

DFT total energy calculations have been performed for ice Ih with different proton distributions, and it has been shown that the energetics of proton ordering differs markedly at the basal and prism surfaces from that in the bulk. Both MC simulations with an empirical potential and a simple Ising model estimate with DFT parameters suggest that the surface will not become fully proton disordered at any temperature before the onset of pre-melting. Structural order parameters, C_{OH}^B and C_{OH}^P, that correlate with the surface energies on basal and prism

faces, have also been defined and the correlations have been explained using a simple electrostatic model based on the interaction between the dangling OH bonds on the surface.

In terms of proton distributions at the basal surface Buch *et al* [12] came to a somewhat similar conclusion to the one arrived at here based on simulations with empirical potentials. Specifically, they concluded that the lowest energy surfaces were those which corresponded to Fletcher's striped phase (figure 4(A)). We agree with this conclusion, however, our DFT calculations further show that this striped structure is just one of many $C_{OH}^B = 2.0$ surfaces that possess similar surface energies. For example, other $C_{OH}^B = 2.0$ surfaces include the one shown in figure 4(B) or the 'glide-twin' and 'mirror-twin' boundary structures reported by Fletcher [11]. All of these surfaces yield surface energies within ca. 1 meV Å^{-2} of each other, well within the likely errors of our computational set-up and exchange–correlation functionals used. Thus, as we have said already, it is not possible to identify any one surface termination as 'the' most stable one, although striped phase domains may be consistent with minor diffraction peaks measured in helium diffraction data and sum frequency generation spectra as discussed by Buch *et al* [12].

We have presented DFT calculations for the surface energies of the ice Ih basal and prism faces. These quantities are difficult to determine in ultra-high vacuum experiments and our DFT calculations suggest a value between 9.7 meV Å^{-2} (BLYP) and 12.2 meV Å^{-2} (PBE) at the temperature of 0 K. On the prism surface a PBE value of 12.0 meV Å^{-2} has been obtained, marginally smaller than the PBE value on the basal plane. These small values for the surface energies are similar to those found for certain layered aluminosilicates such as kaolinite [50] and in terms of meV/(H$_2$O in top half bilayer) consistent with the fact that cleavage of the surface involves the rupture of one hydrogen bond per water in the top half bilayer. Although the precise or 'exact' value of the surface energy is not yet known, we do not expect that it will differ considerably from the range of values obtained here. From the theoretical perspective, its determination will require the application of approaches much more sophisticated than those employed here such as MP2 or quantum Monte Carlo. We note, however, that the very recent PBE0 calculation of an anti-ferroelectric ice XI surface is an important next step in that direction [51]. The surface energy obtained in that study was 0.252 J m^{-2} (15.7 meV Å^{-2}), ca 30% larger than the equivalent PBE value obtained here. On a separate point, it would be very interesting to use the values of the surface energies for the prism and basal surfaces obtained here along with similar surface energy determinations for other relevant ice surfaces such as the secondary prism surface to make a theoretical prediction for the equilibrium crystal shape of ice. However, given the extremely small differences between the surface energies of the various surfaces and the inaccuracies inherent in our GGA calculations it would be imprudent at this stage to make any such predictions. Nonetheless, assuming the surfaces are not kinetically trapped in metastable disordered states, it almost goes without saying, that surface proton order effects are expected to influence the equilibrium shapes obtained.

It is likely that on a macroscopic crystal facet there will be a distribution in the order parameters. Some regions may have high concentrations of dangling OH groups ('hot patches'), which may be more reactive to adsorbates or may melt first upon heating because of a high 'local' surface energy. Indeed, MD simulations suggest that the onset of pre-melting is sensitive to surface proton distribution [30], but more extensive systematic studies of the dependence of melting on C_{OH} are required, which may also reveal that other properties, e.g. surface diffusion [52], are sensitive to the degree of local order or disorder. Finally, this work demonstrates that when constructing ice Ih surfaces for simulation studies the Bernal–Fowler–Pauling ice rules alone are not sufficient since they will lead to ice surfaces with fully random and unrealistically high energy arrangements of dangling OH groups. Instead, an additional constraint of $C_{OH}^B = 2$ on basal faces and $C_{OH}^P = 0$ on prism surfaces is recommended.

Acknowledgments

References

[1] Molina M J, Tso T-L, Molina L T and Wang F C-Y 1987 *Science* **238** 1253
[2] Libbrecht K G 2005 *Rep. Prog. Phys.* **68** 855
[3] Rosenberg R 2005 *Phys. Today* **58** 50
[4] Li Y and Somorjai G A 2007 *J. Phys. Chem. C* **111** 9631
[5] Faraday M 1933 *Faraday's Diary* vol IV (London: Bell and Sons)
[6] Materer N, Starke U, Barbieri A, Van Hove M A, Somorjai G A, Kroes G-J and Minot C 1995 *J. Phys. Chem.* **99** 6267
[7] Materer N, Starke U, Barbieri A, Van Hove M A, Somorjai G A, Kroes G-J and Minot C 1997 *Surf. Sci.* **381** 190
[8] Braun J, Glebov A, Graham A P, Menzel A and Toennies J P 1998 *Phys. Rev. Lett.* **80** 2638
[9] Glebov A, Graham A P, Menzel A, Toennies J P and Senet P 2000 *J. Chem. Phys.* **112** 11011
[10] Parent P, Laffon C, Mangeney C, Bournel F and Tronc M 2002 *J. Chem. Phys.* **117** 10842
[11] Fletcher N H 1992 *Phil. Mag. B* **66** 109
[12] Buch V, Groenzin H, Li I, Shultz M J and Tosatti E 2008 *Proc. Natl Acad. Sci. USA* **105** 5969
[13] Pan D, Liu L-M, Tribello G A, Slater B, Michaelides A and Wang E 2008 *Phys. Rev. Lett.* **101** 155703

[14] Bernal J D and Fowler R H 1933 *J. Chem. Phys.* **1** 515
[15] Pauling L 1935 *J. Am. Chem. Soc.* **57** 2680
[16] Singer S J, Kuo J-L, Hirsch T K, Knight C, Ojamäe L and
Klein M L 2005 *Phys. Rev. Lett.* **94** 135701
[17] Knight C, Singer S J, Kuo J-L, Hirsch T K, Ojamäe L and
Klein M L 2006 *Phys. Rev.* E **73** 056113
[18] Hirsch T K and Ojamäe L 2004 *J. Phys. Chem.* B **108** 15856
[19] VandeVondele J, Krack M, Mohamed F, Parrinello M,
Chassaing T and Hutter J 2005 *Comput. Phys. Commun.*
167 103
[20] Perdew J P, Burke S and Ernzerhof M 1996 *Phys. Rev. Lett.*
77 3865
[21] Becke A D 1988 *Phys. Rev.* A **38** 3098
[22] Lee C, Yang W and Parr R C 1988 *Phys. Rev.* B **37** 785
[23] Sprik M, Hutter J and Parrinello M 1996 *J. Chem. Phys.*
105 1142
[24] Santra B, Michaelides A and Scheffler M 2007 *J. Chem. Phys.*
127 184104
[25] Santra B, Michaelides A, Fuchs M, Tkatchenko A,
Filippi C and Scheffler M 2008 *J. Chem. Phys.* **129** 194111
[26] Goedecker S, Teter M and Hutter J 1996 *Phys. Rev.* B **54** 1703
[27] Nada H and van der Eerden J P 2003 *J. Chem. Phys.* **118** 7401
[28] Sanz E, Vega C, Abascal J L and MacDowell L G 2004 *Phys.
Rev. Lett.* **92** 255701
[29] Carignano M A, Shepson P B and Szleiefer I 2005 *Mol. Phys.*
103 2957
[30] Bishop C L, Pan D, Liu L-M, Tribello G A, Michaelides A,
Wang E and Slater B 2009 *Faraday Discuss.* **141** 277
[31] Rick S W and Haymet A D J 2003 *J. Chem. Phys.* **118** 9291
[32] Feibelman P J 2008 *Phys. Chem. Chem. Phys.* **10** 4688

[33] Cota E and Hoover W G 1977 *J. Chem. Phys.* **67** 3839
[34] Hayward J A and Reimers J R 1997 *J. Chem. Phys.* **106** 1518
[35] Tribello G A and Slater B 2006 *Chem. Phys. Lett.* **425** 246
[36] Fukazawa H, Ikeda S, Oguro M, Bennington S M and
Mae S 2003 *J. Chem. Phys.* **118** 1577
[37] Strässle T, Saitta A M, Klotz S and Braden M 2004 *Phys. Rev.
Lett.* **93** 225901
[38] Thürmer K and Bartelt N C 2008 *Phys. Rev.* B **77** 195425
[39] Feibelman P J 2002 *Science* **295** 99
[40] Petrenko V F and Whitworth R W 1999 *Physics of Ice*
(New York: Oxford University Press)
[41] Makkonen L 1997 *J. Phys. Chem.* B **101** 6196
[42] van Oss C J, Giese R F, Wentzek R, Norris J and
Chuvilin E M 1992 *J. Adhes. Sci. Technol.* **6** 503
[43] Reuck A V S 1957 *Nature* **179** 1119
[44] Douillard J M and Henry M 2003 *J. Colloid Interface Sci.*
263 554
[45] Henry M 2003 *Solid State Sci.* **5** 1201
[46] Bussolin G, Casassa S, Pisani C and Ugliengo P 1998 *J. Chem.
Phys.* **108** 9516
[47] Tasker P W 1979 *J. Phys. C: Solid State Phys.* **12** 4977
[48] Kuo J-L, Ciobanu C V, Ojamäe L, Shavitt I and
Singer S J 2003 *J. Chem. Phys.* **118** 3583
[49] Wannier G H 1950 *Phys. Rev.* **79** 357
[50] Hu X L and Michaelides A 2008 *Surf. Sci.* **602** 960
[51] Labat F and Pouchan C 2009 *Phys. Chem. Chem. Phys.*
11 5833
[52] Nie S, Bartelt N C and Thürmer K 2009 *Phys. Rev. Lett.*
102 136101